Emergent myxobacterial behaviors arise from reversal suppression induced by kin contacts

Rajesh Balagam[1]#, Pengbo Cao[2]#‡, Govind P. Sah[2]#‡, Zhaoyang Zhang[1]#,
Daniel Wall[2]*, Oleg A. Igoshin[1]*

[1] Department of Bioengineering and Center for Theoretical Biological Physics, Rice University, Houston, TX

[2]Department of Molecular Biology, University of Wyoming, 1000 E University Avenue, Laramie, WY

#These authors contributed to this work equally; listed alphabetically.

*Authors to whom correspondence should be addressed; dwall2@uwyo.edu and igoshin@rice.edu

‡**Present addresses:** Pengbo Cao**,** School of Biological Sciences, Georgia Institute of Technology, Atlanta, GA, 30332, USA; Govind P. Sah, Department of Pathology, University of California, 9500 Gilman Drive, La Jolla, CA, USA.

Abstract

A wide range of biological systems – from microbial swarms to bird flocks, display emergent behaviors driven by coordinated movement of individuals. To this end, individual organisms interact by recognizing their kin and adjusting their motility based on others around them. However, even in the best-studied systems, the mechanistic basis of the interplay between kin recognition and motility coordination is not understood. Here, using a combination of experiments and mathematical modeling, we uncover the mechanism of an emergent social behavior in *Myxococcus xanthus*. By overexpressing the cell surface kin recognition receptors, TraA and TraB, large numbers of cells adhere to one another and form organized macroscopic circular aggregates that spin clockwise or counterclockwise. Mechanistically, TraAB adhesion results in sustained cell-cell contacts that signal the Frz chemosensory pathway. In turn, cell reversals are suppressed and circular aggregates form as the result of cells' ability to follow cellular slime trails. Furthermore, our *in-silico* simulations demonstrate a remarkable ability to predict self-organization patterns when phenotypically distinct strains are mixed. Therefore, this work provides key mechanistic insights into *M. xanthus* social interactions and demonstrates how social recognition transforms physical interactions into emergent collective behaviors.

Significance

In many species, large populations exhibit emergent behaviors whereby all related individuals move in unison. For example, fish in schools can all dart in one direction simultaneously avoiding a predator. Currently, it is impossible to explain how such animals recognize kin and elicit these behaviors at a molecular level. However, microbes also recognize kin and exhibit emergent collective behaviors that are experimentally tractable. Here, using a model social bacterium, we engineer dispersed individuals to organize into synchronized collectives that create emergent patterns. With experimental and mathematical approaches we explain how this occurs at both molecular and population levels. The results demonstrate how the combination of local physical interactions and signaling between cells leads to emergent behavior on a global scale.

Introduction

Living systems display remarkable spatial organization patterns from molecules to cells to populations (1, 2). These patterns are a hallmark of emergent behaviors whereby complex functions arise from simple local interactions. For instance, at the cellular level, we have a relatively good understanding of neuron function, but how a collection of neurons integrates into a functional brain is poorly understood. In other cases, emergent behaviors are driven by coordinated movement of system parts, as seen in the collective motion of insect swarms or bird flocks. Inherent in these processes is the ability of individuals to recognize their kin and adjust their movements relative to others around them. Despite much interest in emergent behaviors, the molecular and mechanistic basis of the interplay between kin recognition and the coordination of movements is poorly understood.

The Gram-negative gliding bacterium *Myxococcus xanthus* is a leading model for studying the molecular basis of microbial kin recognition and, separately, for understanding how cells coordinate their movements (3, 4). These microbes are unusually social and exhibit numerous emergent behaviors. Among these are the formation of traveling wave patterns, termed ripples, in which millions of cells self-organize into periodic, rhythmically moving bands (5-7) and, under starvation conditions, aggregate into multicellular fruiting bodies (8, 9). Notably, these emergent social behaviors form from incredibly diverse microbial populations in soil (10), where *M. xanthus* employs kin discrimination to assemble clonal populations or fruiting bodies (11-13). Central to these social behaviors is the ability of cells to control their direction of movement. These long rod-shaped cells tend to align in dense populations (8, 14) and move along their long axis periodically reversing their motion polarity – head becomes tail and vice versa. The frequency of the reversals is mediated by the Frz chemosensory signal transduction pathway (4). Although much progress has been made in myxobacteria biology, a comprehensive and broadly accepted model that explains their self-organization behaviors and kin discrimination is lacking.

One system *M. xanthus* uses to discriminate against non-kin is based on outer membrane exchange (OME) (12). Here, cells recognize their siblings through cell-cell contacts mediated by a polymorphic cell surface receptor called TraA and its cohort protein TraB. TraAB functions as an adhesin, and cells that express identical TraA receptors adhere to one another by homotypic binding, while cells with divergent receptors do not (15, 16). Following TraA-TraA recognition cells bidirectionally exchange outer membrane proteins and lipids (17). The exchange of diverse cellular cargo, including polymorphic toxins, plays a key role in kin discrimination and facilitating cooperative behaviors (18-20). For these, among other reasons, TraAB-mediated OME in myxobacteria serves as a promising model for emergent behavior control, however, whether and how this actually occurs is unknown.

In this study, we investigate the interplay between TraAB-mediated cellular adhesion and motility coordination. Specifically, elevated cell-cell adhesion forces through overexpression of TraAB drive emergent behaviors involving coordinate movements of thousands to millions of cells. To mechanistically understand this emergent behavior, we recapitulated these behaviors in agent-based simulations that mathematically and mechanistically elucidate how these new behaviors emerge. Our work also connects these insights into a newly discovered signal that directs coordinated movements. We propose that the signal arises following sustained cell-cell contacts mediated by TraAB adhesins that suppress cellular reversals, allowing millions of cells to move as a uniform collective.

Results

TraAB overexpression creates emergent circular aggregate behavior.

TraAB cell surface receptors govern allele-specific cell-cell adhesion. When TraAB was overexpressed, cells adhered both end-to-end and side-by-side during shaker flask cultivation (Fig. 1) (15, 18). As myxobacteria are motile on surfaces by adventurous (A) and social (S) gliding motility (21), we sought to understand if TraAB-mediated adhesion affects their collective movements. To clearly assess the impact of cellular adhesion on emergent group behaviors, TraAB adhesin was overproduced in an A^+S^- background, since S-motility promotes extracellular matrix production that complicates analysis. When these cells (hereafter TraAB OE cells) were placed on agar, they displayed an emergent behavior, where thousands of cells self-organized into macroscopic circular aggregates (CAs) (Fig. 1). Initial signs of CAs were easily seen 4 h after cell plating and were prominent by 8-12 h (Fig. S1A and Movie S1). Following extended incubation periods, CAs enlarged to millimeters in diameter with each containing millions of cells. In contrast, the parent strain (A^+S^-, here referred to as wild type (WT)) does not form CAs. Using a different strain with inducible *traAB* expression, CAs were only seen when cells were grown with an inducer (Fig. S1B). Superficially, CAs resemble precursor aggregates that form into fruiting bodies upon starvation-induced development (22), but here TraAB OE cells were grown on rich media, which blocks development. Therefore, without engaging in a complex developmental lifecycle, TraAB

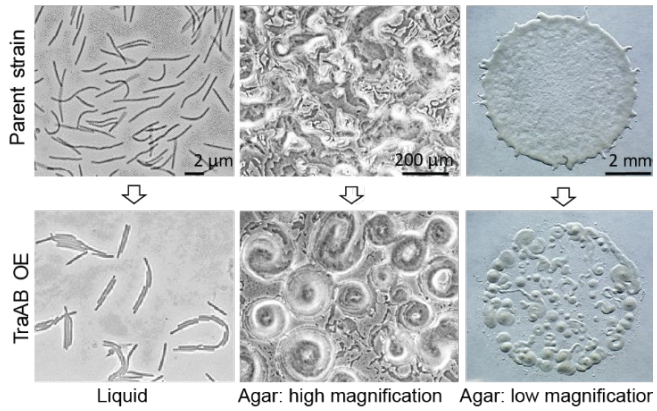

Fig. 1. Emergent behavior triggered by TraAB overexpression (OE). Cells adhere from shaker flask growth (left panel), while on agar surfaces motile populations form circular aggregates (CA) when grown on rich media (middle/right panels, 12 h growth). For simplicity, cells only contain one functional gliding motility system.

overexpression provides a simple and tractable system to assess the impacts of local cell-cell interactions on emergent group behaviors.

The biophysical model reveals CAs only arise from non-reversing agents

To understand mechanistically how CAs emerge in a TraAB OE strain, we attempted to replicate this behavior *in silico* using a biophysical modeling framework that can properly account for forces between cells. To this end, we started with the biophysical model developed by Balagam et al. (23). In this model, to simulate flexible rod-shaped cells, each agent was represented by 7 nodes connected by springs. Agents align with one another on collisions (14) and follow paths left by other agents. These biologically relevant paths are called slime trails, a poorly defined material deposited by gliding *M. xanthus* cells (24, 25). Previously, this model was shown to result in CA formation when the slime-trail following was strong and cells did not reverse (14). Notably, physical adhesion between agents was not required in that model of CA formation. However, in light of our experimental findings (Fig. 1), it seemed that TraAB adhesive forces directed CA formation.

To further assess the role of physical adhesion on emergent behavior, we introduced end-to-end and/or side-by-side adhesion into our model (see SI for details). The simulation results indicated that the addition of adhesion forces by itself does not promote the formation of CAs when agents have periodic reversals (WT cells reversal period ~8 min, (26)). Instead agents self-organized into a network of connected streams (Fig. 2A), with patterns resembling those without adhesion (14). These simulated patterns also resemble experimental observations of the parent strain (Fig. 1, top middle panel). Notably, a further increase in the strength of adhesive forces does not lead to CAs in the population of reversing agents. Instead, excessive adhesion forces exceeding those generated by the agent's motors resulted in unrealistic bending of agents (Fig. 2B). On the other hand, non-reversing agents in our simulations self-organized into CAs either in the absence (Fig. 2C) or in the presence (Fig. 2D) of adhesion. By varying the reversal frequency of agents we show that CAs only begin to appear when the reversal period exceeds ~70 min, i.e. about 10-fold reversal suppression relative to WT was required for the emergence of CAs (Fig. 2E). Comparing the emergent patterns in Figs. 2C-D, we conclude that in our model side-to-side and end-to-end adhesions *per se,* do not

significantly affect the emergent patterns. On the other hand, in addition to suppressed reversals, the ability of agents to lay and follow slime trails was critical (Fig. 2F). As a group of cells moves unidirectionally along such trails, the natural fluctuation in their trajectories leads these paths to close on themselves and leads to the nucleation of CAs. As other cells join these circular paths, CAs grow. Thus, our simulations predict that long reversal periods were necessary for CA formation and therefore we predict that TraAB OE cells must somehow alter cellular reversals. However, to date, no connection between TraAB levels and reversal control was known.

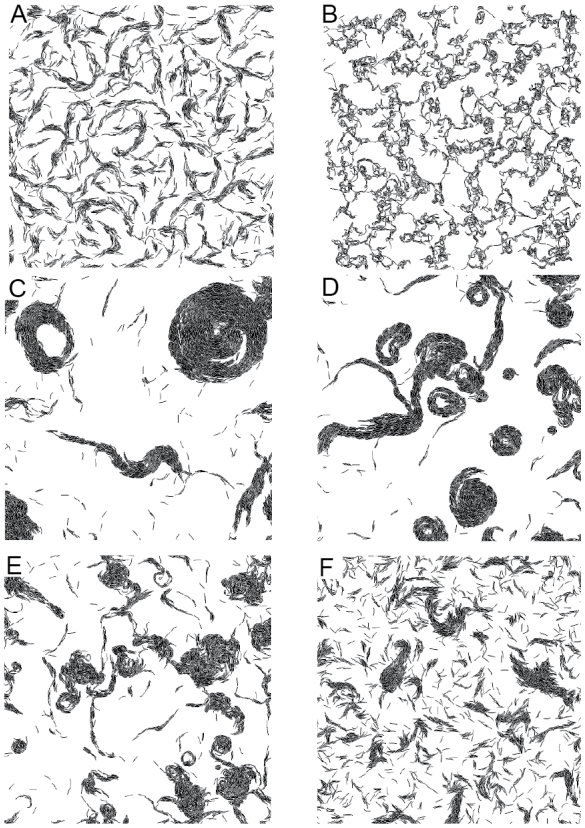

Fig. 2. Biophysical model predicts non-reversing and slime-following agents required for CA formation. (A) Reversing agents do not form CAs in the presence of adhesion or (B) with adhesion forces stronger then motor forces. (C) Non-reversing agents form CAs even in the absence and (D) in the presence of adhesion. (E) Reversing agents with long reversing periods (70 min) initiate CA formation. (F) Non-reversing agents without slime-following do not form CAs.

Cells in CAs suppress reversals

To experimentally test the model prediction, we tracked the movement of single cells within CAs. To this end, a small fraction of TraAB OE cells were fluorescently labeled and mixed with isogenic unlabeled cells (Fig. S2). Cell movements were recorded by time-lapse microscopy (Movie S2) and the tracks and reversals were quantified as in (8). Figure 3A shows the compiled trajectories of these cells with different (random) colors assigned to individual cells. These trajectories reveal that inside CAs all cells move in the same direction around the center of each aggregate. The CAs themselves rotated in either a clockwise or counterclockwise direction (Fig. S2 and Movie S2). Importantly, when the reversal period was quantified over 80% of tracked cells had reversal periods greater than the duration of the movie (> 55 min, Fig. 3B). These results were consistent with our simulation predictions that cell reversals were indeed inhibited within CAs.

Reversal suppression and CAs are dependent on cell-cell adhesion and independent of OME

To determine whether reversal suppression was dependent on cell-cell adhesion or simply due to the TraAB proteins being expressed at elevated levels, the reversal frequencies of isolated cells were also tracked. Here, isolated TraAB OE cells were found not to suppress their reversals compared to controls (Fig. S3). Additionally, given that TraAB mediates OME, whereby bulk protein and lipid cargo are bidirectional transferred between cells (17), raised the possibility that reversal suppression, and hence CA formation, was the result of hyper-active OME. To address this possibility, the OmpA domain from TraB was deleted, resulting in a strain producing functional TraAB adhesins, but defective in OME (Fig. S4A, B). Importantly, this strain similarly formed CAs, albeit at reduced levels (Fig. S4C). We conclude that sustained cell-cell contacts mediated by TraAB OE, but not OME, suppresses cellular reversals.

Reversal suppression acts through the Frz pathway and is critical for CA formation

Cellular reversals in *M. xanthus* are controlled by a 'chemosensory' signal transduction pathway called Frz (4). Similar to other Che pathways from enteric bacteria, the Frz pathway contains a methyl-accepting chemotaxis protein (MCP) called FrzCD, however, it is cytoplasmic and lacks typical transmembrane and ligand-binding domains. To test whether reversal suppression within CAs was controlled by the Frz pathway, we evaluated the FrzCD methylation state as a measure of Frz signaling (27, 28). Here, TraAB OE cells that developed CAs were harvested from agar plates and compared to its parent strain similarly prepared. Importantly, the western blot showed the relative proportions of four FrzCD bands varied between cells from CAs versus those that were not (Fig. 3C). This result indicated different FrzCD methylation states, and hence different Frz signaling activity, between the TraAB OE and parent strains. To further test the role of Frz, we added very low concentrations of a chemical (isoamyl alcohol), which acts as a repellant that triggers cell reversals via the Frz pathway (27, 29), to agar media and assessed what happened to a TraAB OE strain. Importantly, in a dose-dependent manner CA formation was abolished (Fig. S5). Finally, based on our simulations (Fig.

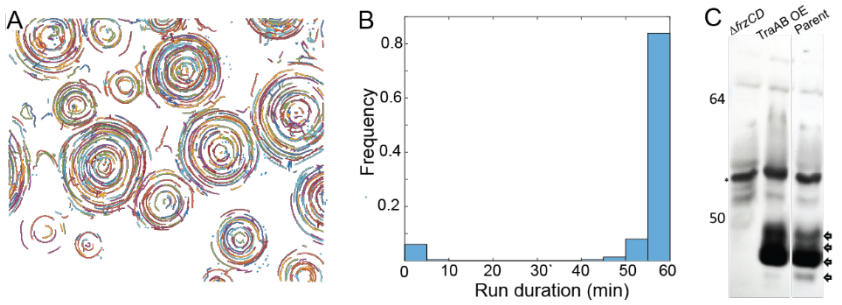

Fig. 3. TraAB OE suppresses cell reversals via Frz chemosensory pathway. (A) Digitally labeled trajectories of marked cells from Movie S2. Each colored curve represents a trajectory of one cell. (B) Run duration distribution of labeled cells. Total experiment time 60 min, 1 min intervals; note, most cells do not reverse during the 60 min duration. (C) CAs correlate with FrzCD activation. Isogenic strains that formed CAs or not (parent) were harvested and FrzCD mobility was analyzed on SDS-PAGE 6-15% gradient gels that were immunoblotted with FrzCD polyclonal antibodies. Representative blot shown; left, molecular weight standards (kDa); *non-specific cross-reacting protein serves as a loading control; arrows mark discrete FrzCD bands.

2C) and prior work (30), we tested and found that Frz non-reversing mutants also form CAs (Fig. S6), although not as distinct as TraAB OE cells. We conclude that modulating reversal frequency via the Frz pathway plays a key role in CA formation.

The biophysical model suggests that contact-dependent reversal suppression lead to CA formation

To reconcile the differences in reversal frequencies between groups of cells (Fig. 3B) and individual cells (Fig. S3), and in light of Frz involvement, we hypothesized that a short-range signal arises from sustained cell-cell contacts mediated by TraAB, suppresses cell reversals via the Frz pathway. Consistent with this model, cell density and contact-dependent signals during development are known to regulate reversal frequency (4, 8, 31, 32), and, additionally, myxobacterial ripples originate from cell contact-dependent reversal modulation. To implement this mechanism in our model, we chose a phenomenological approach to simulate contact-dependent reversal suppression inspired by (9). To this end, at each time step when a given agent was in contact with another agent, its reversal clock was reset backward by a fixed amount. Given that TraAB stimulates both end-to-end and side-to-side adhesion (Fig. 1), we assumed either one or both interactions lead to reversal suppression. We hypothesized that adhesion forces that hold agents together will increase reversal suppression by physically increasing the contact duration. To differentiate WT cell-cell contacts at high-cell densities from those that occur between TraAB OE cells, we introduced a time delay between agent adhesion events and reversal suppression signaling. That delay was set at 5 min to ensure no CAs formed in WT strain simulations as explained below.

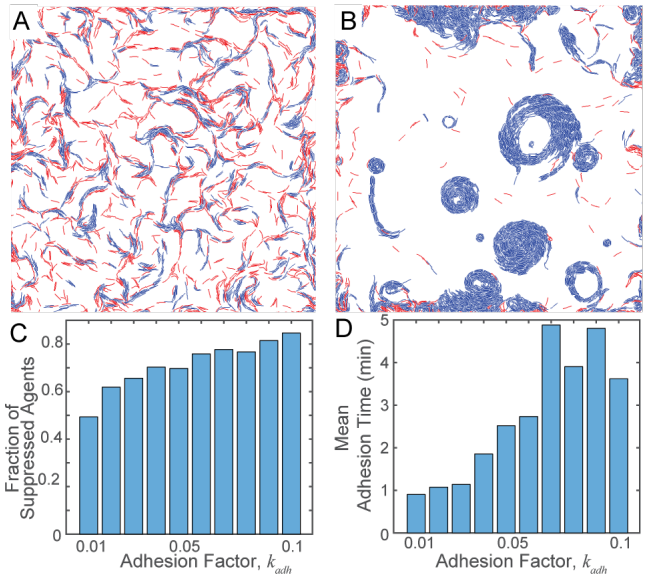

Fig. 4. Strong adhesion and cell contact-dependent reversal suppression results in CAs in simulations. (A) Agents with weak adhesion (WT phenotype) show only a small number engaging in reversal suppression (blue) with no emergent behavior. Agents with no reversal suppression are red. (B) Stronger adhesion leads to prevalent reversal suppression (blue) and formation of CAs. (C) Fraction of agents with suppressed reversals as a function of adhesion strength at end of the simulation. (D) Average adhesion bond time at the final 10 min of simulation. The adhesion factor k_{adh} is defined in SI. WT, $k_{adh} = 0.01$; OE, $k_{adh} = 0.1$.

In the presence of the signaling delay, with only weak adhesion (representing the parent strain with low TraAB levels; Fig. 4A), agent interactions were short, and reversals were not substantially inhibited, resulting in normal patterns (compare with Fig. 2A). As shown, less than half of the agent contacts lasted

213 long enough to produce reversal suppression. Next, we performed a simulation of agents with stronger and
214 consequently longer adhesion events and as a result, the frequency of reversal suppression was dramatically
215 increased (Fig. 4B). Under these conditions, CAs readily formed, and in agreement with experiments,
216 showed the unidirectional rotation of agents in a clockwise or counter-clockwise direction (Movie S3). This
217 result supports our hypothesis that reversal suppression was necessary for CA formation. Furthermore, our
218 simulations found that when adhesion strength gradually increases from WT to TraAB OE levels the
219 number of agents participating in contact signaling gradually increased (Fig. 4C). However, the effect of
220 the adhesion strength on the duration of adhesion (time before adhesion bond broke) was more dramatic
221 (Fig. 4D). Therefore, to ensure our simulations were consistent with the lack of CAs in the WT strain, we
222 assumed the transient contacts that were shorter than 5 min in the simulations do not suppress reversals.
223 This threshold was important because CAs would form even with weak adhesion in its absence (Fig. S7).

224 Notably, the behaviors on individual agents in our model match the trends for experimentally tracked cells.
225 With tracking data, we quantified how cell speed and angular speed change as a function of distance to an
226 aggregate center. The experimental results demonstrate that cell speed increases while angular speed
227 decreases as a function of distance from the aggregate center (Fig. S8A, B). Similarly, by quantifying agent
228 speed and angular speed in simulations as a function of distance to the aggregate centers (Fig. S8C, D), we
229 demonstrated that trends were qualitatively consistent with experimental observations.

230 The contact-mediated reversal suppression model accurately predicts emergent patterns of 231 multi-strain mixtures

232 To further interrogate our model and computationally investigate the interplay between the kin recognition
233 and emergent patterns, we conducted simulations where two types of agents were mixed. In the first
234 simulation, agents overexpressed TraAB receptors of different types (alleles). These receptors do not match
235 and hence the different type agents cannot adhere to each other (15, 33), and reversal suppression only
236 occurs when two agents of the same type engaged in sustained contact. Initially, we hypothesized that
237 differential adhesion would lead to "phase-separation" between agent types, analogous to phase-separation
238 between oil and water. However, in contrast to this prediction, our simulations found that both agent types
239 were mixed within CAs (Fig. 5A). To explain this result, we suggest that reversal suppression and the ability
240 of agents to follow each other's slime trail overpowered their distinct adhesive forces.

241 Next, to investigate the impacts of heterogeneous cell-cell adhesion forces across populations, we simulated
242 a TraAB OE (green) mixed with a WT (red) agent. These agents contained different adhesive forces. WT
243 had similar weak adhesions between themselves and with TraAB OE agents (15, 16), and hence they were
244 less susceptible to prolonged cell-cell contacts and reversal suppression. In contrast, TraAB OE agents had

strong adhesion among themselves. Interestingly, the simulations showed that the WT agents impeded the formation of CAs by TraAB OE, perhaps by breaking cell-cell adhesions and blocking prolonged contacts that are required for reversal suppression (Fig. 5B, compare to Fig. 4A). Furthermore, to test the role of reversal suppression in CA formation, we conducted a simulation where a TraAB OE agent was mixed with a weakly adhering agent that does not reverse, i.e. a *frz* mutant. Strikingly, in this case, the non-reversing and TraAB OE agents formed mixed CAs together (Fig. 5C). This result again demonstrates the key role reversal suppression plays in the emergent CA behavior.

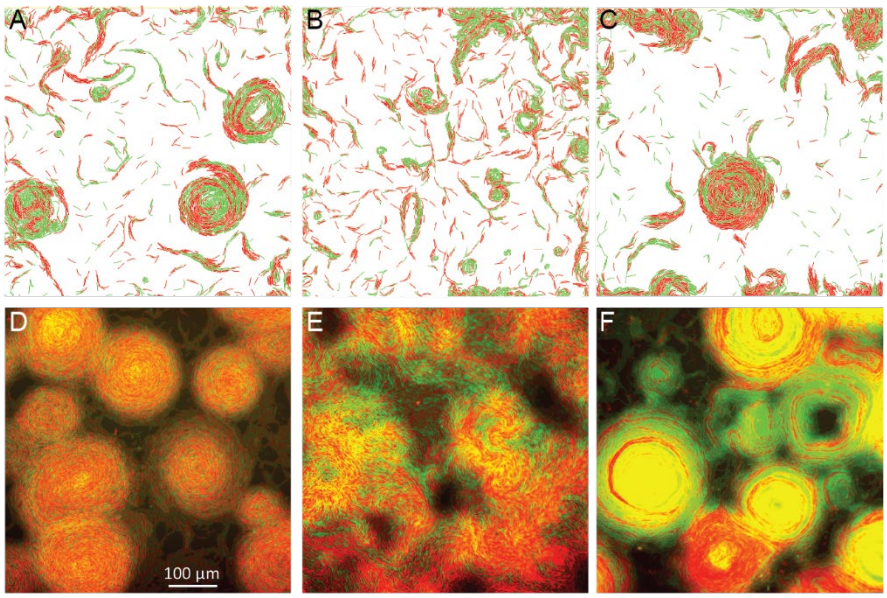

Fig. 5. Correlations between simulations and experiments when different combinations of agents or cells were mixed 1:1. (A) Simulation of two different agents (red and green) that adhere to themselves but not each other. (B) Simulation of adhesive agents (TraAB OE, green) mixed with non-adhesive agents (WT, red). (C) Simulation of adhesive agents (green) mixed with non-adhesive non-reversing agents (red). (D) Experimental mixture of two strains that overexpress different TraA receptors (red and green) that adhere to themselves but not each other. (E) Mixture of TraAB OE strain (green) mixed with a strain that does not adhere (WT, red). (F) Mixture of TraAB OE strain (green) mixed with a non-adhesive non-reversing mutant (red). D-F merged images; see Fig. S10 for single-channel images.

To test our model predictions, we experimentally mixed strains in a manner analogous to simulations. Importantly, for all three strain mixtures, experimental results showed CA patterns or lack thereof, that correlated with all three corresponding simulations (Fig. 5, compare A-C to D-F). Additionally, the degree that strains did or did not mix also correlated with simulation outcomes. Specifically, we found that: (i) Introduction of cells with low cell adhesion capabilities (e.g. WT) blocked the emergence of CAs by apparently disrupting prolonged cell-cell adhesions between TraAB OE cells and hence disrupting reversal suppression (Fig. 5E). Moreover, these disruptions were potent because even a minority of such cells, e.g. 7:1 ratio of TraAB OE to WT, blocked CA formation (Fig. S9). (ii) As found in our simulations and above experiments, reversal suppression played a crucial role, because in contrast to mixtures with WT cells (Fig. 5E), when TraAB OE cells were mixed 1:1 with Frz non-reversing mutants, which express TraAB at wild-type levels, CAs readily formed between these strains (Fig. 5F). (iii) When two strains overexpressing incompatible TraA receptors were mixed, they also formed CAs together (Fig. 5D). Therefore, the ability

279 of different strains to strongly adhere to each other was not critical, as long as cell reversals were suppressed,
280 whether by cell-cell adhesion or by *frz* mutations. That is, when divergent populations with suppressed
281 reversals were mixed, they readily merged and jointly form CAs by following their reinforced slime trails.

282 Discussion

283 Emergent behaviors transcend the properties of individual components and result in complex functions that
284 are often difficult or impossible to understand mechanistically, on the systems level. Here we investigated
285 a tractable emergent behavior, whereby thousand to millions of cells form spinning CAs. By using
286 experimental and biophysical agent-based modeling, we elucidated the underlying mechanism.
287 Unexpectedly, our models revealed that the formation of CAs only occurs when cellular reversals are
288 suppressed. Experiments confirmed that reversal suppression is required and showed it is only occurred in
289 dense populations, i.e. upon cell-cell contacts. Using these observations, we hypothesized that reversals
290 were suppressed by long-lasting cell contacts that adhesins stabilized. This model is supported by several
291 experimental findings, including altered FrzCD methylation patterns of TraAB OE cells from CAs, showing
292 that reversal suppression acts via the Frz pathway. Our model not only explained the differences in patterns
293 between WT and TraAB OE cells but also qualitatively matches how actual cellular linear and angular
294 speeds change within CAs. Furthermore, our model accurately predicted emergent patterns when
295 phenotypically distinct strains were mixed.

296 A longstanding and central question in the myxobacterial field is what physiological signal does the Frz
297 pathway perceive (4)? Our results provide insights to this question by revealing that sustained cell-cell
298 contacts generate an intracellular signal, perceived by Frz, which suppresses cellular reversals. Consistent
299 with this model, FrzCD proteins were previously found to transiently align between cells upon cell-cell
300 contact (34). Although the details of such a signal remain abstruse, we suggest an undiscovered factor (e.g.
301 protein) recognizes these cell-cell engagements and then interacts with FrzCD. This hub protein is already
302 known to interact with two CheW-like proteins (FrzA and FrzB), a CheA-Y hybrid protein (FrzE), a
303 methyltransferase (FrzF), and a methylesterase (FrzG) (4). Since FrzCD is an unusual MCP that lacks a
304 ligand-binding domain (27, 35), to perceive an input signal it must interact, either directly or indirectly,
305 with another protein(s) that serves as the signal receiver. Such candidates include one of the other 20 MCPs
306 in the *M. xanthus* genome (28, 36), proteins that contain domains commonly associated with cytoplasmic
307 MCPs, e.g. PAS domains (35), or by a novel mechanism. Future studies need to identify this factor.

308 It also remains to be determined whether the mechanism responsible for CAs is similar to how cells form
309 spherical fruiting bodies during starvation-induced development, where cell reversals are again suppressed
310 (8). Although TraAB proteins are not required for fruiting body formation, the Frz pathway is (4), and thus

other mechanisms that stabilize cell-cell contacts during development may activate the same signal to suppress reversals described here. It also remains to be seen if collision-induced reversals that were shown (7, 9) to be responsible for rippling are triggered by the same pathway, i.e. by the disruption of reversal-suppressing cell contacts. Notably, the formation of CAs in our model only requires the ability of cells to lay and follow slime trails as well as adhesion to stabilize cell-cell contacts, thereby leading to reversal suppression. That is, for non-reversing agents (or strains), the formation of CAs is not significantly affected by adhesion forces on their own. This conclusion is supported by the observation that Frz non-reversing mutants form CAs (Fig. S6 and (30)), which confirms TraAB-driven cell adhesion is required for reversal suppression rather than for the formation of CA *per se*. In contrast, another theoretical study (37) showed that non-reversing agents could also form CAs by instead invoking a short-range active guiding mechanism. In this model, agents do not follow slime trails, but instead, generate active guiding forces that allow the lagging agent to seek and maintain a constant distance from the leading agent. This active guiding force is assumed to arise from physical adhesion and/or attraction between cell poles, which could be generated by polar type IV pili. Notably, these models make different predictions on CA dynamics. In one case CAs rotate as rigid bodies (37), whereas CAs based on slime trail following (14) showed a decrease in angular velocity the farther agents were from the aggregate center. These patterns of cell speed and angular velocity from experiments qualitatively match our model predictions and do not match the predictions of (37).

In conclusion, with a synergistic combination of experiments and modeling our work reveals how a kin recognition adhesin mediates a local behavioral change, reversal suppression, which enables an emergent behavior that resembles starvation-induced multicellular development. These discoveries provide an experimental handle to identify the elusive cellular signal that directs the Frz pathway to control cellular reversals. By extension, other systems that contain seemingly complex emergent behaviors, can be broken down and tackled by using a combination of modeling and simplified experimental manipulations to uncover their mechanisms of action.

Acknowledgments

We thank Beiyan Nan for FrzCD antibodies. This work was supported by the National Science Foundation grants DMS- 1903275 and OIS-1951025 (to OAI) and the National Institutes of Health grant GM101449 (to D.W).

340 **References**

341 1. Wingreen NS & Huang KC (2015) Physics of Intracellular Organization in Bacteria. *Annu Rev*
342 *Microbiol* 69:361-379.
343 2. Couzin ID & Krause J (2003) Self-organization and collective behavior in vertebrates. *Advances*
344 *in the Study of Behavior*, ed Peter J.B. Slater JSR, Charles T. Snowdon, Timothy J. Roper
345 (Elsevier Science, San Diego, CA, USA), Vol 32, pp 1-67.
346 3. Wall D (2016) Kin recognition in bacteria. *Annu Rev Microbiol* 70:143-160.
347 4. Zusman DR, Scott AE, Yang Z, & Kirby JR (2007) Chemosensory pathways, motility and
348 development in Myxococcus xanthus. *Nat Rev Microbiol* 5(11):862-872.
349 5. Berleman JE, Chumley T, Cheung P, & Kirby JR (2006) Rippling is a predatory behavior in
350 Myxococcus xanthus. *J Bacteriol* 188(16):5888-5895.
351 6. Welch R & Kaiser D (2001) Cell behavior in traveling wave patterns of myxobacteria. *Proc Natl*
352 *Acad Sci U S A* 98(26):14907-14912.
353 7. Igoshin OA, Mogilner A, Welch RD, Kaiser D, & Oster G (2001) Pattern formation and traveling
354 waves in myxobacteria: theory and modeling. *Proc Natl Acad Sci U S A* 98(26):14913-14918.
355 8. Cotter CR, Schuttler HB, Igoshin OA, & Shimkets LJ (2017) Data-driven modeling reveals cell
356 behaviors controlling self-organization during Myxococcus xanthus development. *Proc Natl Acad*
357 *Sci U S A* 114(23):E4592-E4601.
358 9. Zhang H*, et al.* (2012) The Mechanistic Basis of Myxococcus xanthus Rippling Behavior and Its
359 Physiological Role during Predation. *PLoS Computational Biology* 8(9):e1002715.
360 10. Gans J, Wolinsky M, & Dunbar J (2005) Computational improvements reveal great bacterial
361 diversity and high metal toxicity in soil. *Science* 309(5739):1387-1390.
362 11. Wielgoss S, Wolfensberger R, Sun L, Fiegna F, & Velicer GJ (2019) Social genes are selection
363 hotspots in kin groups of a soil microbe. *Science* 363(6433):1342-1345.
364 12. Sah GP & Wall D (2020) Kin recognition and outer membrane exchange (OME) in
365 myxobacteria. *Curr Opin Microbiol* 56:81-88.
366 13. Vassallo CN, Troselj V, Weltzer ML, & Wall D (2020) Rapid diversification of wild social
367 groups driven by toxin-immunity loci on mobile genetic elements. *ISME J* 14(10):2474-2487.
368 14. Balagam R & Igoshin OA (2015) Mechanism for Collective Cell Alignment in Myxococcus
369 xanthus Bacteria. *PLOS Computational Biology* 11(8):e1004474.
370 15. Cao P & Wall D (2017) Self-identity reprogrammed by a single residue switch in a cell surface
371 receptor of a social bacterium. *Proc Natl Acad Sci U S A* 114(14):3732-3737.
372 16. Cao PB & Wall D (2019) Direct visualization of a molecular handshake that governs kin
373 recognition and tissue formation in myxobacteria. *Nat Commun* 10.

374 17. Pathak DT, *et al.* (2012) Cell contact-dependent outer membrane exchange in myxobacteria:
375 Genetic determinants and mechanism. *PLoS Genet* 8(4):e1002626.
376 18. Vassallo C, *et al.* (2015) Cell rejuvenation and social behaviors promoted by LPS exchange in
377 myxobacteria. *Proc Natl Acad Sci U S A* 112(22):E2939-2946.
378 19. Vassallo CN & Wall D (2019) Self-identity barcodes encoded by six expansive polymorphic
379 toxin families discriminate kin in myxobacteria. *Proc Natl Acad Sci U S A* 116(49):24808-24818.
380 20. Vassallo CN & Wall D (2016) Tissue repair in myxobacteria: A cooperative strategy to heal
381 cellular damage. *BioEssays* 38(4):306-315.
382 21. Nan B & Zusman DR (2011) Uncovering the mystery of gliding motility in the myxobacteria.
383 *Annu Rev Genet* 45:21-39.
384 22. Jelsbak L & Sogaard-Andersen L (2000) Pattern formation: fruiting body morphogenesis in
385 Myxococcus xanthus. *Curr Opin Microbiol* 3(6):637-642.
386 23. Balagam R, *et al.* (2014) Myxococcus xanthus Gliding Motors Are Elastically Coupled to the
387 Substrate as Predicted by the Focal Adhesion Model of Gliding Motility. *PLoS Computational*
388 *Biology* 10(5):e1003619.
389 24. Burchard RP (1982) Trail following by gliding bacteria. *J Bacteriol* 152(1):495-501.
390 25. Ducret A, Valignat MP, Mouhamar F, Mignot T, & Theodoly O (2012) Wet-surface-enhanced
391 ellipsometric contrast microscopy identifies slime as a major adhesion factor during bacterial
392 surface motility. *Proc Natl Acad Sci U S A* 109(25):10036-10041.
393 26. Berleman JE, Chumley T, Cheung P, & Kirby JR (2006) Rippling Is a Predatory Behavior in
394 Myxococcus xanthus. *Journal of Bacteriology* 188(16):5888-5895.
395 27. Bustamante VH, Martinez-Flores I, Vlamakis HC, & Zusman DR (2004) Analysis of the Frz
396 signal transduction system of Myxococcus xanthus shows the importance of the conserved C-
397 terminal region of the cytoplasmic chemoreceptor FrzCD in sensing signals. *Mol Microbiol*
398 53(5):1501-1513.
399 28. Xu Q, Black WP, Cadieux CL, & Yang Z (2008) Independence and interdependence of Dif and
400 Frz chemosensory pathways in Myxococcus xanthus chemotaxis. *Mol Microbiol* 69(3):714-723.
401 29. McBride MJ, Kohler T, & Zusman DR (1992) Methylation of FrzCD, a methyl-accepting taxis
402 protein of Myxococcus xanthus, is correlated with factors affecting cell behavior. *J Bacteriol*
403 174(13):4246-4257.
404 30. Starruss J, *et al.* (2012) Pattern-formation mechanisms in motility mutants of Myxococcus
405 xanthus. *Interface Focus* 2(6):774-785.
406 31. Jelsbak L & Sogaard-Andersen L (2002) Pattern formation by a cell surface-associated
407 morphogen in Myxococcus xanthus. *Proc Natl Acad Sci U S A* 99(4):2032-2037.

408 32. Shi W, Ngok FK, & Zusman DR (1996) Cell density regulates cellular reversal frequency in
409 Myxococcus xanthus. *Proc Natl Acad Sci U S A* 93(9):4142-4146.
410 33. Cao P, Wei X, Awal RP, Muller R, & Wall D (2019) A highly polymorphic receptor governs
411 many distinct self-recognition types within the Myxococcales order. *mBio* 10(1).
412 34. Mauriello EM, Astling DP, Sliusarenko O, & Zusman DR (2009) Localization of a bacterial
413 cytoplasmic receptor is dynamic and changes with cell-cell contacts. *Proc Natl Acad Sci U S A*
414 106(12):4852-4857.
415 35. Collins KD, Lacal J, & Ottemann KM (2014) Internal sense of direction: sensing and signaling
416 from cytoplasmic chemoreceptors. *Microbiol Mol Biol Rev* 78(4):672-684.
417 36. Moine A*, et al.* (2014) Functional organization of a multimodular bacterial chemosensory
418 apparatus. *PLoS Genet* 10(3):e1004164.
419 37. Janulevicius A, Van Loosdrecht M, & Picioreanu C (2015) Short-Range Guiding Can Result in
420 the Formation of Circular Aggregates in Myxobacteria Populations. *PLOS Computational*
421 *Biology* 11(4):e1004213.

422

Supplemental Materials:

Emergent myxobacterial behaviors arise from reversal suppression induced by kin contacts

Rajesh Balagam[1]#, Pengbo Cao[2]#‡, Govind P. Sah[2]#‡, Zhaoyang Zhang[1]#, Daniel Wall[2]*, Oleg A. Igoshin[1]*

[1] Department of Bioengineering and Center for Theoretical Biological Physics, Rice University, Houston, Texas [2]Department of Molecular Biology, University of Wyoming, 1000 E University Avenue, Laramie, WY, USA.

#These authors contributed to this work equally; listed alphabetically. *Authors to whom correspondence should be addressed; dwall2@uwyo.edu and igoshin@rice.edu

Present addresses: Pengbo Cao**,** School of Biological Sciences, Georgia Institute of Technology, Atlanta, GA, 30332, USA; Govind P. Sah, Department of Pathology, University of California, 9500 Gilman Drive, La Jolla, CA, USA.

Supporting Text: Materials and methods

Bacterial strains and growth conditions

All strains used in this study are listed in Table S1. *M. xanthus* cells were routinely grown in CTT medium (1% [w/v] Casitone; 10 mM Tris-HCl, pH 7.6; 1 mM KH_2PO_4; 8 mM $MgSO_4$) in the dark at 33 °C. 1.5% (w/v) agar was added to the medium to make plates. To prepare agarose pads for microscopy, Casitone was reduced to 0.2% (w/v), and 1% (w/v) agarose was added to the medium. *E. coli* strains were routinely cultured in LB medium at 37 °C. As needed for antibiotic selection or protein induction, 50 μg ml^{-1} of kanamycin (Km), 10 μg ml^{-1} oxytetracycline, or 1 mM IPTG was added to media.

Plasmid and strain construction

All plasmids and primers are listed in Table S1 and S2. To maximize the expression of TraAB adhesin, pPC57 was constructed where the native GTG start codon of *traA* was changed to ATG and TraAB expression is driven by a heterologous *pilA* promoter (P_{pilA}). This site-directed mutagenesis was done by using primers containing the desired mutation, and the amplified *traAB* fragments were ligated into pDP22 (linearized with XbaI and HindIII) with T4 DNA ligase. To achieve inducible overexpression of TraAB (pPC58), *traAB* fragments were PCR amplified and then ligated into pMR3487 (linearized with XbaI and KpnI) through Gibson Assembly (New England Biolabs). To create pPC59, primers were designed to amplify fragments of *traAB* and omit the region encoding for OmpA, and the resulting fragments were ligated into XbaI and HindIII digested pDP22 through Gibson Assembly. Plasmid construction was done in *E. coli* TOP10. All plasmids were verified by PCR, restriction enzyme digestion, and if necessary, by DNA sequencing. To construct *M. xanthus* strains, plasmid or chromosomal DNA was electroporated into cells and integrated into the chromosome by site-specific or homologous recombination. For pSWU19 derived plasmids integration occurs at the Mx8 attachment site, while pMR3487 recombines at another site and expression is induced with IPTG (1).

Aggregate formation

M. xanthus cells were grown to logarithmic growth phase in CTT, washed with TPM buffer (CTT without Casitone), and resuspended to the calculated density of 5×10^8 cells per mL. 5 μL of cell suspension was then spotted onto 1/2 CTT (CTT medium with 0.5% Casitone) agar plates supplemented with 2 mM $CaCl_2$. In some cases, different strains were mixed at desired ratios before spotting. Spots were air-dried and plates were then incubated at 33 °C overnight before imaging. To assess the impacts of cellular reversals on CA formation, isoamyl alcohol (IAA) of different concentrations was supplemented to agar media.

Microscopy

CA formation on agar plates was imaged using a Nikon E800 phase-contrast microscope (10× phase-contrast objective lens coupled to a Hamamatsu CCD camera and Image-Pro Plus software), or an Olympus IX83 inverted microscope (10× objective lens coupled to a ORCA-Flash 4.0 LT sCMOS camera and cellSens software), or an Olympus SZX10 stereomicroscope (low magnification coupled to a digital imaging system). To track isolated cell reversals, cells were mounted on an agarose pad and imaged with a 20× phase-contrast objective lens. Fluorescence microscopy was used to track individual cells within CAs with a 10× lens objective and a Texas Red filter set. Cell-cell adhesion was imaged directly from overnight cultures mounted on glass slides with a 100× oil immersion objective lens.

Immunoblot

Western analysis was performed as previously described with modifications (2). Briefly, equal amounts of cell extract were loaded on a 15 cm gradient gel (6-15%) and proteins separated by SDS-PAGE. Following transfer blots were probed with primary polyclonal rabbit FrzCD sera at a 1:25,000 dilution. For detection,

HRP-conjugate goat-anti-rabbit secondary antibody was used (1:20,000 dilution, Pierce) and developed with SuperSignal West Pico Plus chemiluminescent substrate (Thermo Scientific).

The Agent-Based-Simulation framework

The simulation model framework is adapted from our previous work (3, 4). A brief description of the previous model, simulation framework as well as the new changes introduced in the framework are presented below. All of the parameters are summarized in Table S3. Each agent is represented as a connected string of N (= 7) circular nodes with a total cell length L (= 6 μm) and width w (= 0.5 μm) (see figure S1 in (4) and additional details in (3)). Neighboring circular nodes are kept at a fixed distance apart by (N-1) rectangular spacers. Neighboring circular nodes and rectangular spacers are connected by linear (spring constant, k_l) and angular (spring constant, k_b) springs. Linear springs here resist elongation and compression of cell nodes. The linear spring constant is managed by the model engine to keep the agent length constant. Angular springs resist bending from straight-line configuration to simulate elastic bending behavior of *M. xanthus* cells.

Each agent moves forward by the propulsive forces. Since the experiments are done with the cells lacking S-motility, we only implement gliding (A) motility of *M. xanthus* cells based on distributed force generation model (5-8). At each node i a propulsion force ($\boldsymbol{F}_{p,i} = F_T/(N-1), F_T$ is the total propulsive force) is applied in the current travel direction towards the neighboring node. Viscous drag forces ($\boldsymbol{F}_d$) arising from the surrounding fluid/slime act on nodes opposing their movement with the force proportional to the velocity or each node with proportionality coefficient c (drag coefficient).

Agent movement is affected by collisions, periodic reversals, random turns, and slime-trail-following by agents. Collisions in our model are resolved by applying repulsion forces on nodes that keep agents from overlapping. Further, adhesive attachments between the agent and the underlying cell substrate (based on focal adhesion of model of gliding motility in *M. xanthus* (7)) at each node resist lateral displacement of the nodes during collisions with other cells. These attachments are modeled as linear springs (spring constant, k_a) and are detached at a threshold distance $d_{a,max}$. For each agent, the first and last nodes in the current cell travel direction are designated as head and tail nodes respectively. Periodic reversals in our model are introduced by switching the roles of head and tail nodes and reversing the propulsive force direction at the inner nodes. Reversals in agents are triggered asynchronously by an internal timer expiring at the end of the reversal period (τ_r) after which the timer is reset to zero. *M. xanthus* cells exhibit random turns during movement on solid surfaces (4). These random turns are added to the model by changing the direction of the propulsive force on the head node of the agent by 90° (either clockwise or anti-clockwise chosen randomly) for a fixed amount of time (1 min) at regular time intervals (τ_t) triggered another internal timer. Slime-trail-following by *M. xanthus* cells is a known phenomenon (9), in which cells leave a slime trail on the substrate and other cells crossing these trails later start following them. We added slime-trail-following of agents in our model using a phenomenological approach where we gradually change the direction of propulsive force ($\boldsymbol{F}_p$) on the head node of the agent parallel to the direction of slime trail ($\hat{e}_s$) it is currently crossing. (see (3) for implementation details of slime-trail-following mechanism in our model).

Cell adhesion

To simulate adhesive interactions between agents, we apply lateral adhesive forces (F_{adh}) on nodes of neighboring agents if the two nodes are closer than a specific threshold distance. In the simulation, we include end-end adhesion where one agent's head node is attached to another agent's tail node and lateral

adhesion where an agent is attached to a nearby agent side by side. The threshold distance for lateral adhesion $d_{thr} = 0.9$ µm and for end-end adhesion $d_{thr} = 1.5$µm. This is because we assume the cell wall/membrane can be stretched more along the long axis.

We use the following equation to calculate cell adhesion force:

$$F_{adh} = \begin{cases} 0 & d > d_{thr} \\ k_{adh} \dfrac{d - w}{w} F_T & d_{thr} > d > w \end{cases}$$

Here, d is the distance between neighboring nodes, w is the width of cells, k_{adh} is the adhesion force factor describing the ratio of the maximal adhesive force to the total propulsive force of the agent F_T. For OE cells, $k_{adh} = 0.1$ for WT cells $k_{adh} = 0.01$. These adhesive forces are applied on each node in the direction towards the neighbor node center.

Reversal suppression induced by cell contacts

In the model, cell reversal is controlled by a reversal clock in the agent, if the reversal clock records a time longer than the chosen reversal period, the reversing happens and the reversal clock is reset to 0. In this work, we assume if the adhesion lasts longer than a threshold time (τ_{thr}, set to be 5 min unless indicated otherwise), agents suppress their reversals. We set the threshold to be 5 minutes. When suppression of reversal happens, the reversal clock is slowed down or even turned back for every time step that agents remain in contact past the threshold. For each agent, we calculate the total suppression from end-end pairs and lateral suppression contacts, i.e.:

$$r_{t+1} = \begin{cases} \max(r_t + dt(1 - \sum_{\substack{\text{end-end} \\ \text{pairs}}} \delta R_e - \sum_{\substack{\text{lateral} \\ \text{pairs}}} \delta R_l), \quad 0) & if\ r_t < \tau_r \\ 0 & if\ r_t \geq \tau_r \end{cases}$$

Here, r_t is reversal clock at time step t, r_{t+1} is reversal clock at time step $t + 1$, τ_r is reversal period, δR_e is end-end reversal suppression factor, δR_l is lateral reversal suppression factor and dt is the time step.

Simulation of the mixed agent population

To simulate mixed populations of two types of agents, we assign each agent a label that corresponds to the strain it represents. We use WT label for parent strain, OE for TraAB-expression, and NR for non-reversing. Adhesion interactions are assumed to be 10x stronger ($k_{adh} = 0.1$) if both agents have OE labels as compared to all other pairs ($k_{adh} = 0.01$). For simulations of mixture OE agents of different TraAB alleles, no adhesion between agents with different alleles is occurring ($k_{adh} = 0$), thus the reversal suppression also will not happen. Since in our model adhesion is required for reversal suppression, these interactions do not affect reversals.

Simulation procedure

The simulation procedure here is similar to (3). We study collective behaviors of cells by simulating mechanical interactions among a large number (M) of agents on a 2D simulation region with periodic boundary conditions in an agent-based framework.

We initialize agents one by one on a square simulation region (dimension L_{sim}) over few initial time steps until desired cell density (η) is reached. Agents are initialized in random positions over the simulation region with their orientations (θ) chosen randomly in the range $[0, 2\pi]$. Agent nodes are initialized in the

straight-line configuration. During initialization, agent configurations that overlap with existing agents are rejected. After initialization, the head node for each agent is chosen between its two end-nodes with 50% probability.

At each time step of the simulation, agents move according to the various forces acting on their nodes. Changes in node positions and velocities are obtained by integrating the equations of motion based on Newton's laws. We use the Box2D physics library (10, 11) for solving the equations of motion and for effective collision resolution. Snapshots of the simulation region, the orientation of each agent, and its node positions are recorded every minute for later analysis.

Simulations are implemented in Java programming language with a Java port of Box2D library (http://www.jbox2d.org/). The parameters of the simulation are shown in table S1. Other parameters of the model are the same as in (3, 4). Each simulation is run for 250 min. The codes and datasets are available in the https://github.com/Igoshin-Group/CircularAggregatesPaper1 repository.

157 **Table S1** Plasmids and strains used in this study

Plasmids	Relevant features	Figure(s) used	Source
pCV10	pSWU19-P_{R3+4}-eGFP, Km^r		(12)
pDP21	P_{pilA}-*traAB* in pSWU19 (Mx8 *attP*), Km^r		(13)
pDP22	P_{pilA} in pSWU19, Km^r		(14)
pMR3487	IPTG-inducible promoter, Tc^r		(1)
ptdTomato	pMR3487-*tdTomato*, Tc^r		Larry Shimkets
pPC4	P_{pilA}-$traAB^{Mf}$ in pSWU19, Km^r		(15)
pPC57	P_{pilA}-(ATG)-*traAB* in pSWU19, Km^r		This study
pPC58	pMR3487-(ATG)-*traAB*, Tc^r		This study
pPC59	P_{pilA}-(ATG)-*traAB*(ΔOmpA) in pSWU19, Km^r		This study
Strains			
TOP10	*E. coli* cloning strain		Invitrogen
DK1622	Wild-type *M. xanthus*; all strains derived		(16)
DK8601	DK1622 *aglB1* (*aglQ1*) Δ*pilA*::tc, nonmotile, Tc^r	1 top/left panel	(16, 17)
DW1463	DK8601 (pDP21), Km^r, Tc^r	1 bottom left panel	(13, 17)
DK10410	DK1622 Δ*pilA* (markerless)	1 top middle/right panels, 3C, S1A, S3, S5, S9, Movie S1	(13, 18)
DW2292	DK10410 (pPC57), Km^r	1 bottom middle/right panels, 3A, 3B, S1A, S2, S3, S4A, S4C, S5, S6, S8A, S8B, S9, Movies S1-S2	This study
DW2293	DW2292 (ptdTomato), Km^r, Tc^r	3A, 3B, S2, S8A, S8B, Movie S2	This study
DW2294	DK10410 (pPC58), Tc^r	3C, S1B	This study
DW712	DK1622 Δ*frzA-E*::km Δ*pilA*::tc, Km^r, Tc^r	S6	This study
DW1466	DK1622 Δ*cglC* Δ*tgl* (markerless)	S4B	(13)
DW1483	DK8601 Δ*traAB* (markerless)	S4B	(13, 15)
DW2296	DW1463 (pPC57), Km^r, Tc^r	S4B	This study
DW2297	DW1483 (pPC59), Km^r, Tc^r	S4B	This study
DW2298	DW2270 (pPC59), Km^r	S4A, S4C	This study
DW2270	DK10410 Δ*traAB* (markerless)	S4A, S4C	(19)
DW2295	DK10410 (ptdTomato), Tc^r	5E, S10	This study
DW2539	DW2294 Δ*frzA-E*::km, Km^r, Tc^r	3C	This study
DW2538	DW2295 Δ*frzA-E*::km, Km^r, Tc^r	5F, S10	This study
DW2300	DW2270 (pPC4, ptdTomato), Km^r, Tc^r	5D, S10	This study
DW2540	DW2294 (pCV10), Km^r, Tc^r	5D, 5E, 5F, S10	This study

158

159

160 **Table S2. Primers used in this study**

Primer name	Sequence (5'→3')
(ATG)-TraA-RBS-XbaI-F	GACGACTCTAGAGGAAACCAAGAATAGAAATAGAAAGGAGAATTAATGGGAGATATCCCTCATTG
TraB-HindIII-R	GACGACAAGCTTGGAGTTCTTCACCTCGGACTC
XbaI-(ATG)-TraA-F	GGATAACAATTAAGGAGGCTCTAGAATGGGAGATATCCCTCATTG
TraB-KpnI-R	TGATTACGAAGGCGAGCTCGGTACCGGAGTTCTTCACCTCGGACT
pSWU19-EcoRI-P_{pilA}-F	AGGAAACAGCTATGACCATGATTACGAATTCCGTCATGTTGGACGAGGT
TraB-ΔOmpA-R	GAAGTCGACGCGGTTGAGCTGCTCCAGGATGACAAT
TraB-ΔOmpA-F	GGAGCAGCTCAACCGCGTCGACTTCACCATCC
pSWU19-XbaI-HindIII-TraB-R	TGCATGCCTGCAGGTCGACTCTAGAAAGCTTGGAGTTCTTCACCTCGGACTC

161 *Restriction sites are underlined.

162

Table S3. Simulation parameters

Description	Symbol	Value
Agent length	L	6 μm (20, 21)
Agent width	W	0.5 μm (20, 21)
Agent mass	m	$1.2 \times 10^{-15}\ kg$
Number of nodes per agent	N	7
Linear spring constant	k_l	Managed by Box2D (10)
Angular spring constant	k_b	$10 pN \cdot \mu m/\mathrm{rad}$ (21-23)
Total propulsive force per agent	F_T	55 pN (4)
Drag coefficient	c	22 $pN \cdot min/\mu m$
Substrate adhesions spring constant	k_a	100 $pN/\mu m$ (4)
Substrate adhesion break distance	$d_{a,max}$	0.5 μm (4)
Reversal period	τ_r	8 min (24)
Direction change period	τ_t	5 min
Simulation region dimension	L_{sim}	200 μm
Agent density	η	0.074 $cell/\mu m^2$
Time-step	dt	0.0067 min
Adhesion force factor	k_{adh}	WT: 0.01, OE: 0.1
End-end suppression factor	δR_e	1
Lateral suppression factor	δR_l	0.04
The minimum time for suppression activation	τ_{thr}	5 min
Maximal adhesion length	d_{thr}	1.5 μm for end-end adhesion 0.9 μm for lateral adhesion

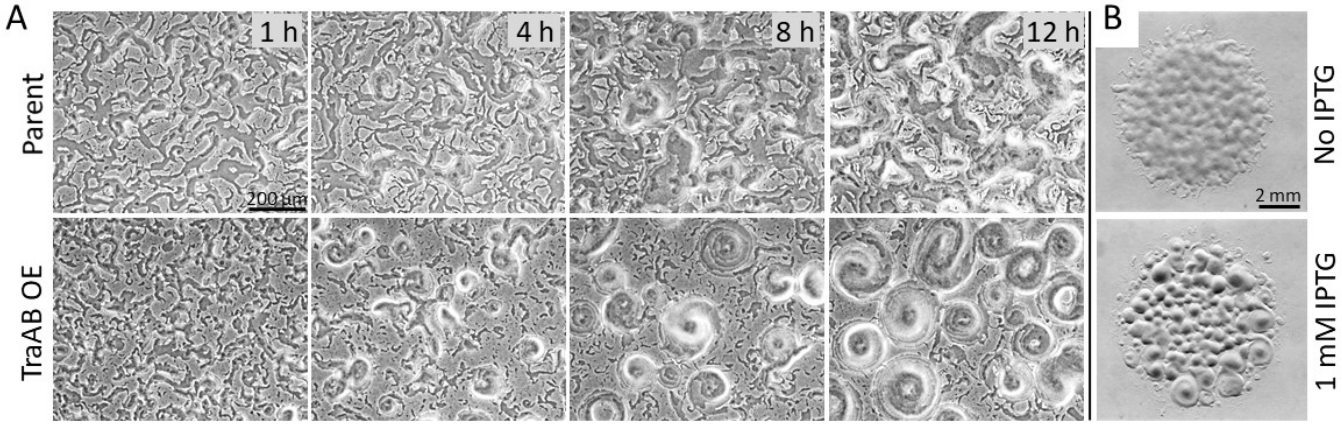

Fig. S1. Induction of CAs**.** (A) Time course after plating of constitutive P_{pilA}-*traAB* OE strain and its parent on agar spotted at low cell densities (3×10^9 cfu/ml). (B) Strain with an inducible promoter (P_{IPTG}-*traAB* OE) plated in the presence and absence of inducer and grown for 36 h.

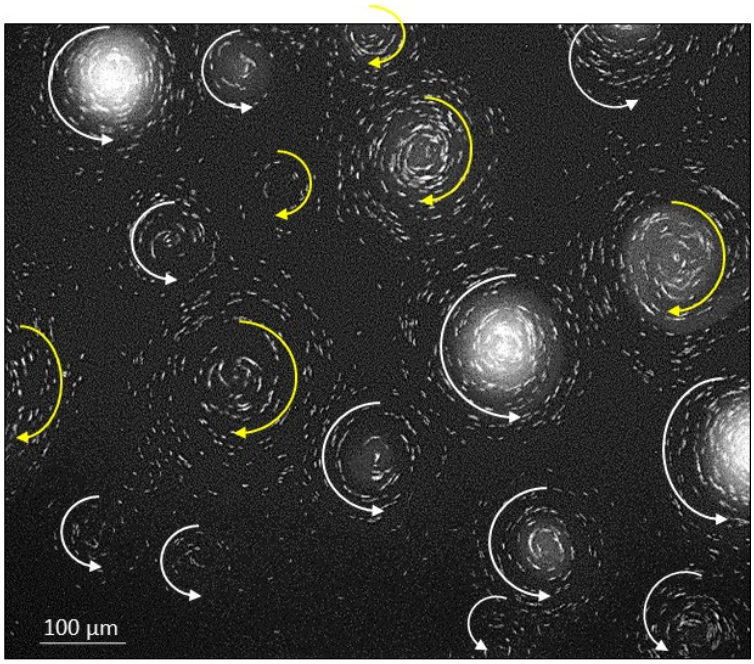

Fig. S2. Fluorescent micrograph of CAs. Labeled and non-labeled cells were mixed 1:250. White arrows indicate counter-clockwise rotations, while yellow arrows indicate clockwise rotation. A time-lapse series is shown in Movie S2.

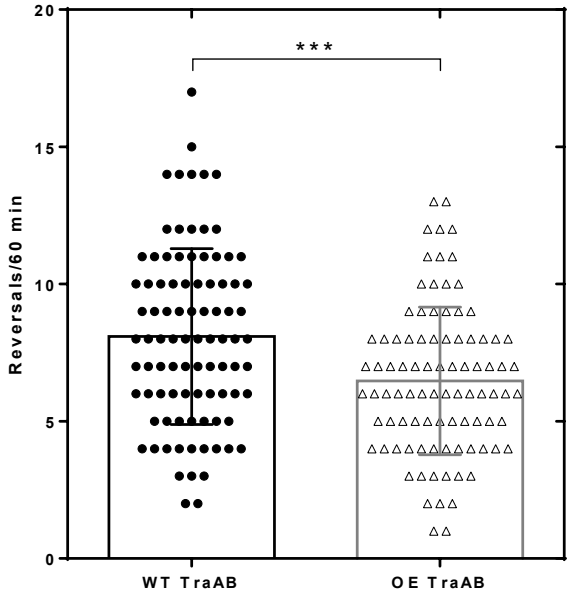

Number of cells	91	91
	8.088	6.473
Std. Deviation	3.203	2.689
P value	0.0003	

178

179 **Fig. S3**. TraAB OE does not suppress cell reversals of isolated cells. Cell movements tracked by time-lapse
180 microscopy in three independent experiments and compared between TraAB OE to WT cells.

181

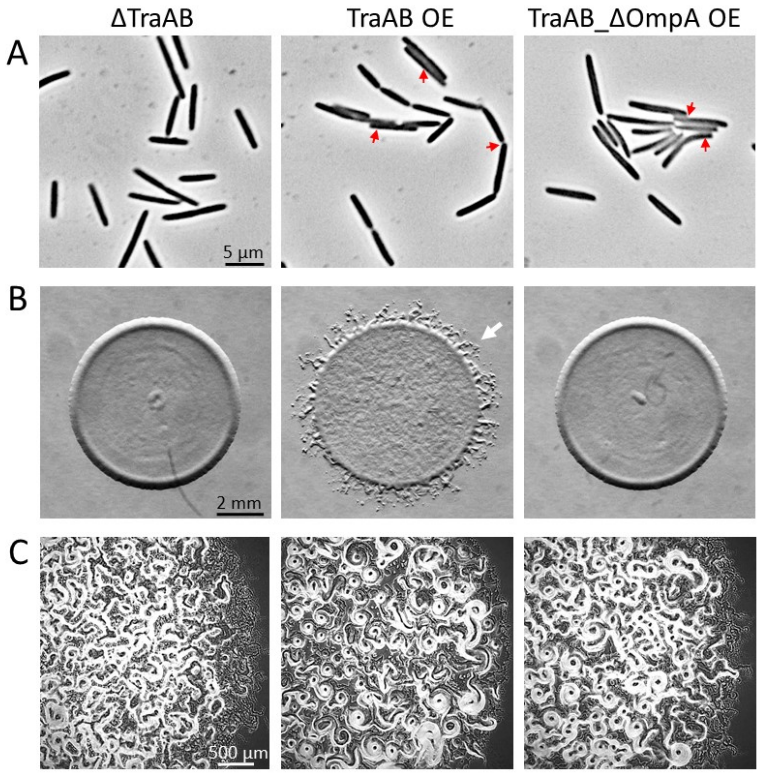

Fig. S4. Outer membrane exchange (OME) is not required for CA formation. (A) Cell-cell adhesion phenotypes (red arrows) of indicated strains. (B) Stimulation assays assess *traAB* allele function in OME. Here, two nonmotile strains were mixed 1:1 and when OME occurs the recipient cells receive missing motility proteins and swarm out from the colony edge (middle panel arrow) (25). When OME is defective the recipient cells remain nonmotile and produce sharp colony edges (left, right panels). (C) Ability of *traAB* alleles to promote CAs (middle, right panels) or not (left panel). See Table S1 for strain details.

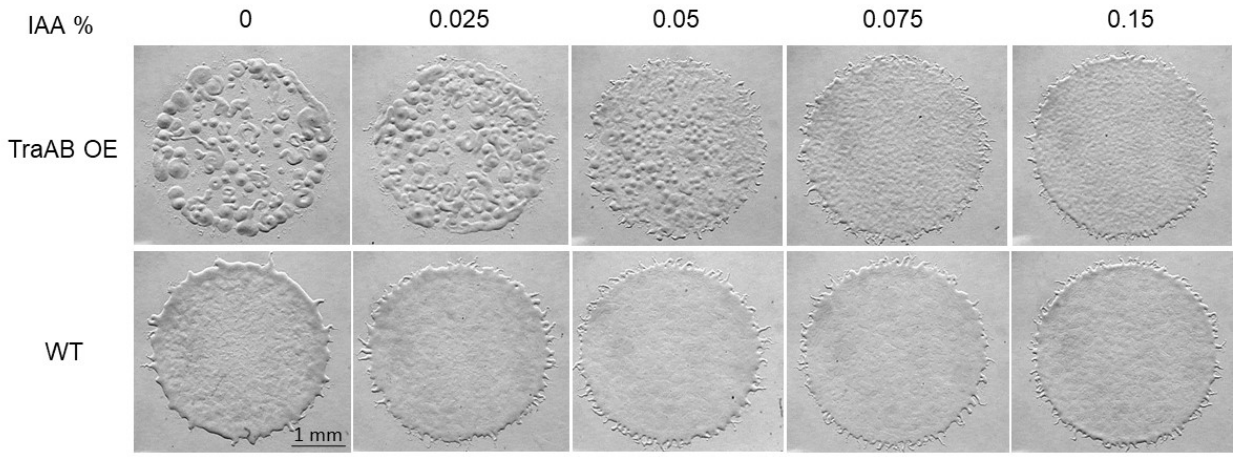

Fig. S5. Chemical induction of cellular reversals blocks CA formation. Isoamyl alcohol (IAA) stimulates cell reversals by triggering the Frz pathway. IAA was added at indicated concentrations to agar media and micrographs taken at 24 h. The two left panels with no IAA are also shown in Fig. 1.

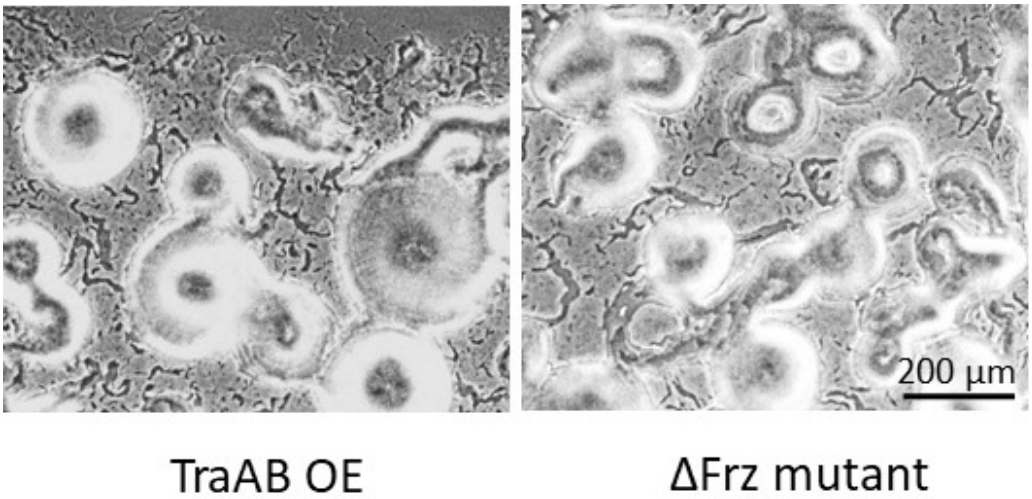

Fig. S6. Frz non-reversing mutant strain forms CAs, though not as distinctive as the TraAB OE strain.

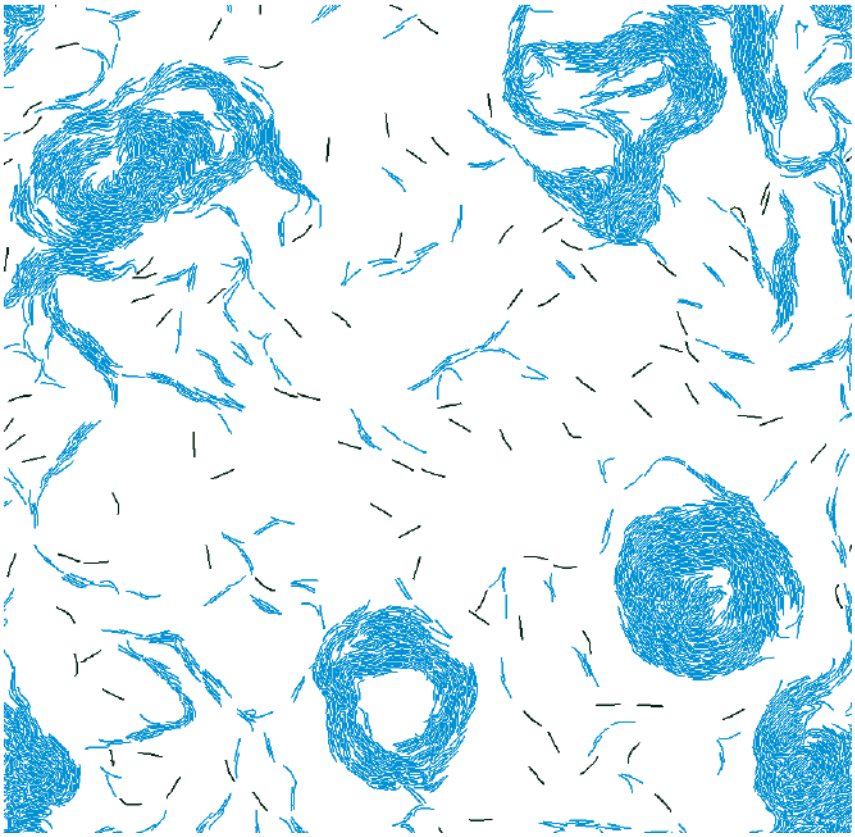

Fig. S7. WT agents without time threshold for reversal suppression form CAs. Black agents not reversal-suppressed; blue agents are reversal-suppressed.

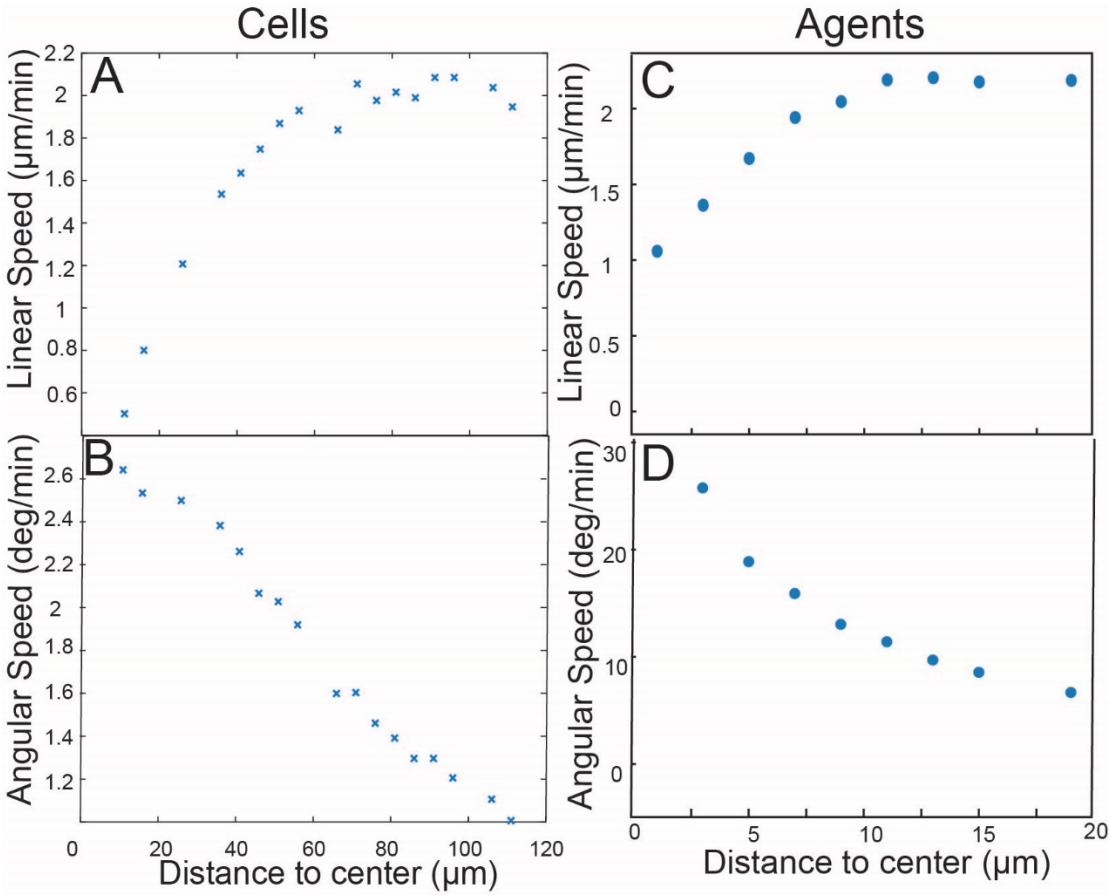

Fig. S8. Linear speed and angular speed as measured experimentally and in simulations. Experimentally determined cell linear speed (A) and angular speed (B) measured as a function of distance to the center from Figure 3A and Movie S2. Each data point represents the average of cells within a 5 μm window. Agent linear (C) and angular speed (D) measured as a function of distance to center from simulations. Each data point represents the average of cells within a 2 μm ring. The data and simulations indicate that the CAs do not rotate as a rigid body, because that is defined as cells having the same angular speed throughout CAs. Note the quantitative agreement between the speed values is not possible because the CAs in the experiment were larger (radius 120 μm) than in the simulation (radius < 20 μm). This discrepancy was mainly due to computational limitations as our simulation can only simulate a limited number of agents in a small simulation domain (200 μm× 200 μm).

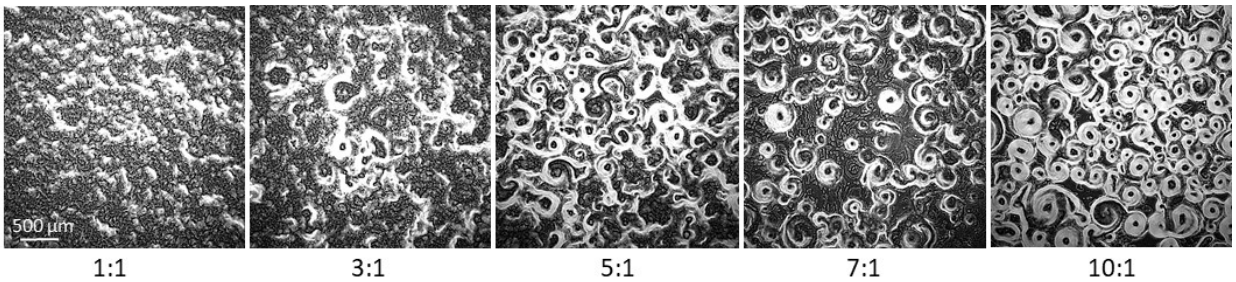

Fig. S9. WT cells inhibit CA formation by TraAB OE. The ratios of TraAB OE to WT are indicated. Micrographs taken at 24 h.

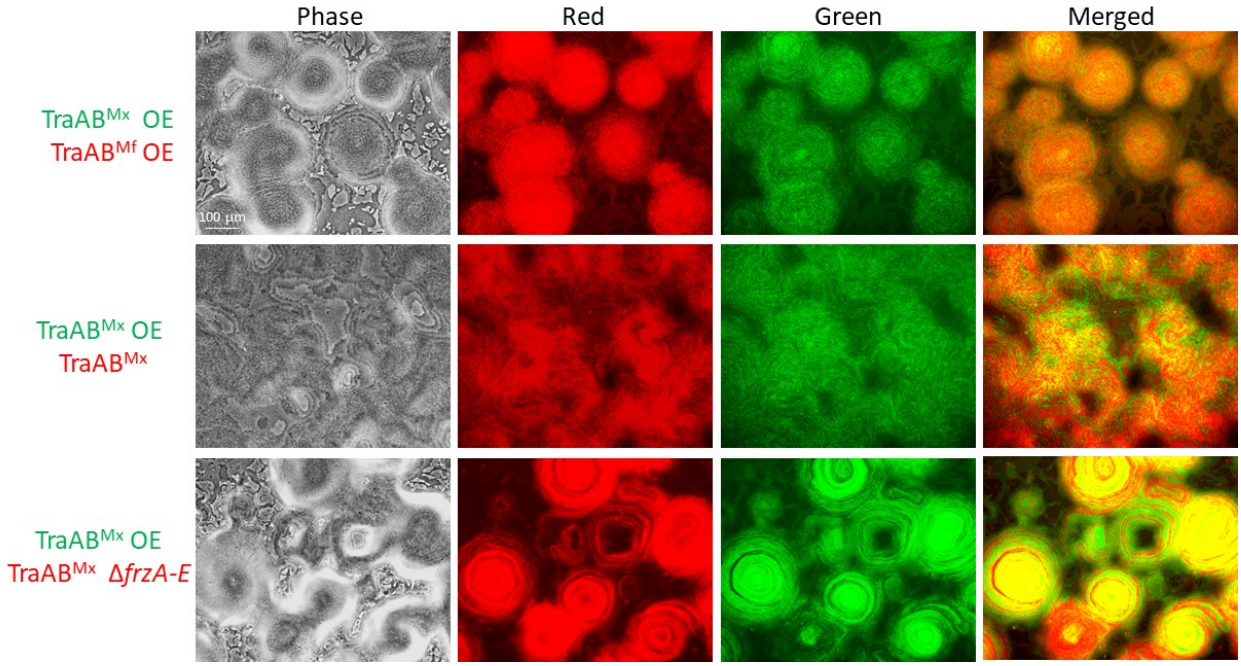

Fig. S10. CA phenotypes of strain mixtures (1:1 ratios) expressing different *traAB* alleles. The panels show single channels and merged images used to create Figure 6D-F panels and strains used. Media included 1 mM IPTG to allow TraAB^{Mx} overexpression (DW2540). See Tables S1 for additional strain details.

226 **Movie S1**: Time-lapse series of strains from Figure S1 at indicated times after cell platings. Time intervals
227 between frames 30 sec; each series for 15 min. See Table S1 for strain details.

228 **Movie S2**. Time-lapse movie that is represented in Figures 3A and S2. Time intervals between frames 1
229 min. See Table S1 for strain details.

230 **Movie S3**. Time-lapse movie from Figure 4B. The movie records the last 60 mins of a 180 min simulation
231 with a different color scheme for better contrast. In each frame, white cells represent reversal-
232 suppressed cells and red cells are not reversal-suppressed.

SI References

1. A. A. Iniesta, F. Garcia-Heras, J. Abellon-Ruiz, A. Gallego-Garcia, M. Elias-Arnanz, Two systems for conditional gene expression in Myxococcus xanthus inducible by isopropyl-beta-D-thiogalactopyranoside or vanillate. *J Bacteriol* **194**, 5875-5885 (2012).
2. G. P. Sah, P. Cao, D. Wall, MYXO-CTERM sorting tag directs proteins to the cell surface via the type II secretion system. *Mol Microbiol* **113**, 1038-1051 (2020).
3. R. Balagam, O. A. Igoshin, Mechanism for Collective Cell Alignment in Myxococcus xanthus Bacteria. *PLOS Computational Biology* **11**, e1004474 (2015).
4. R. Balagam *et al.*, Myxococcus xanthus Gliding Motors Are Elastically Coupled to the Substrate as Predicted by the Focal Adhesion Model of Gliding Motility. *PLoS Computational Biology* **10**, e1003619 (2014).
5. B. Nan, D. R. Zusman, Uncovering the mystery of gliding motility in the myxobacteria. *Annu Rev Genet* **45**, 21-39 (2011).
6. M. Sun, M. Wartel, E. Cascales, J. W. Shaevitz, T. Mignot, Motor-driven intracellular transport powers bacterial gliding motility. *Proceedings of the National Academy of Sciences* **108**, 7559-7564 (2011).
7. T. Mignot, J. W. Shaevitz, P. L. Hartzell, D. R. Zusman, Evidence that focal adhesion complexes power bacterial gliding motility. *Science* **315**, 853-856 (2007).
8. O. Sliusarenko, D. R. Zusman, G. Oster, The motors powering A-motility in Myxococcus xanthus are distributed along the cell body. *J Bacteriol* **189**, 7920-7921 (2007).
9. R. P. Burchard, Trail following by gliding bacteria. *J Bacteriol* **152**, 495-501 (1982).
10. A. P. Pugsley, Translocation of a folded protein across the outer membrane in Escherichia coli. *Proc Natl Acad Sci U S A* **89**, 12058-12062 (1992).
11. E. Catto (2012) Box2D - A 2D physics engine for games.
12. C. N. Vassallo *et al.*, Infectious polymorphic toxins delivered by outer membrane exchange discriminate kin in myxobacteria. *eLife* **6** (2017).
13. D. T. Pathak *et al.*, Cell contact-dependent outer membrane exchange in myxobacteria: genetic determinants and mechanism. *PLoS Genet* **8**, e1002626 (2012).
14. D. T. Pathak, X. Wei, A. Dey, D. Wall, Molecular recognition by a polymorphic cell surface receptor governs cooperative behaviors in bacteria. *PLoS Genet* **9**, e1003891 (2013).
15. P. Cao, D. Wall, Self-identity reprogrammed by a single residue switch in a cell surface receptor of a social bacterium. *Proc Natl Acad Sci U S A* **114**, 3732-3737 (2017).
16. A. Dey *et al.*, Sibling rivalry in *Myxococcus xanthus* is mediated by kin recognition and a polyploid prophage. *J Bacteriol* **198**, 994-1004 (2016).
17. D. Wall, D. Kaiser, Alignment enhances the cell-to-cell transfer of pilus phenotype. *Proc Natl Acad Sci U S A* **95**, 3054-3058 (1998).
18. S. S. Wu, D. Kaiser, Regulation of expression of the pilA gene in Myxococcus xanthus. *J Bacteriol* **179**, 7748-7758 (1997).
19. P. B. Cao, D. Wall, Direct visualization of a molecular handshake that governs kin recognition and tissue formation in myxobacteria. *Nat Commun* **10** (2019).
20. H. Zhang *et al.*, The Mechanistic Basis of Myxococcus xanthus Rippling Behavior and Its Physiological Role during Predation. *PLoS Computational Biology* **8**, e1002715 (2012).
21. A. Janulevicius, M. C. M. Van Loosdrecht, A. Simone, C. Picioreanu, Cell Flexibility Affects the Alignment of Model Myxobacteria. *Biophysical Journal* **99**, 3129-3138 (2010).
22. C. W. Harvey *et al.*, Study of elastic collisions of Myxococcus xanthus in swarms. *Phys Biol* **8**, 026016 (2011).
23. C. W. Wolgemuth, Force and Flexibility of Flailing Myxobacteria. *Biophysical Journal* **89**, 945-950 (2005).
24. J. E. Berleman, T. Chumley, P. Cheung, J. R. Kirby, Rippling Is a Predatory Behavior in Myxococcus xanthus. *Journal of Bacteriology* **188**, 5888-5895 (2006).

283 25. D. T. Pathak, D. Wall, Identification of the *cglC*, *cglD*, *cglE*, and *cglF* genes and their role in cell
284 contact-dependent gliding motility in *Myxococcus xanthus*. *J Bacteriol* **194**, 1940-1949 (2012).

285